P. MYŚLIWIEC*, R.E. ŚLIWA*#, R. OSTROWSKI*

FRICTION STIR WELDING OF ULTRATHIN AA2024-T3 ALUMINUM SHEETS USING CERAMIC TOOL

The paper presents the results of research work on linear FSW (Friction Stir Welding) joining aluminum alloys AA2024-T3 of 0.5 mm in thickness. The study was conducted on properly adapted numerical controlled 3 axis milling machine using a ceramic tool and special designed fastening device. The tool dimensions have been estimated according to the algorithm shown in the literature [4]. All joints were made of end-to end (butt) configuration under different welding speed. The rotational speed of the tool and tool offset was constant. The effect of selected technological parameters on the quality of the joint was analyzed. Produced butt joint have been subjected to a static tensile testing to identify mechanical features of the materials of joints compared to parent materials. Measurements of micro hardness HV in the plastically formed stir zone of joint and in the parent material have been carried out. Axial and radial welding forces in the joining region were recorded during the tests and their dependency from the welding parameters was studied. Based on the results of strength tests the efficiency of joints for sheets of 0.5 mm in thicknesses oscillated up to 96% compared to the parent material. It has been found that for given parameters the correct, free of defects joints were obtained. The paper also presents the results of low-cycle fatigue tests of obtained FSW joints. The use of a ceramic tool in the FSW process allows to obtain welds with higher strength than conventional tools. The results suggests that FSW can be potentially applied to joining aluminum alloys.

Keywords: friction stir welding, aluminum alloys, ceramic tools, FSW force measurements, low-cycle fatigue test, FSW joint durability

1. Introduction

Friction stir welding (FSW) is a solid-state joining process. It involves rotating a cylindrical tool with a short protrusion or "pin", which is plunged between two metal plates (Fig. 1) [1]. High pressure and shear strain plastically deform and consolidate the work pieces by means of material extrusion from the front to the back of the tool . The plates are clamped with a sturdy fixture to the backing plate with an anvil piece of hardened steel underneath the path of the FSW tool, counteracting the vertical and horizontal forces arising during welding. The combination of frictional and deformation heating around the immersed rotating pin and at the interface between the shoulder of tool and the plates leads to the consolidation of the two metal plates as the tool traverses along the joint line. FSW was invented in the Welding Institute (TWI) in the UK in 1991 by Wayne Thomas and has been researched extensively since then and applied in various fields such as the automotive, marine, and aerospace industries, where aluminum alloys are heavily used [1,2]. Global trends in CO_2 emission and gas price have attracted extensive attentions from the automotive manufacturing industry to produce lighter, safer and environmental friendly vehicles [3].

In conventional FSW, a tool consisting of a probe and a shoulder was commonly used. In general, the diameter of the shoulder is about three times bigger than that of the probe [4]. However, this type of tool is associated with several issues. One is the significant through-thickness temperature gradient because the heat generated by the shoulder is much higher than that by the probe, with the peak temperature developing at the top surface, which affects joint microstructure and properties. Another issue is the generation of the flash and arc corrugation because some plastic material moves out of the weld [5].

Many studies have been conducted to understand the weld characteristics of Al alloys using friction stir welding (FSW) since it was presented by Thomas et al. [1]. For instance, Colligan [6] characterized the material flow of Al alloys in FSW by using a tracer material. Xu et al. [7] developed two finite-element models to predict the material flow during the FSW of Al alloys. Mishra and Ma [8] described the current state of understanding and development of FSW. Fujii et al. [9] demonstrated the influence of tool geometry, welding parameters, and joint configurations on material flow and temperature distribution in FSW. Vijayan and Raju [10] outlined the detailed parameters governing the joining process, including the rotation rate, welding speed, axial force, and tool geometry. Kulkarni et al. [11] investigated the influence of the type of the backing plate material on weld quality. Balasubramanian et al. [12] widely presented observations about forces occurring during the FSW process.

* RZESZOW UNIVERSITY OF TECHNOLOGY, DEPARTMENT OF MATERIAL FORMING AND PROCESSING, 12 POWSTAŃCÓW WARSZAWY AV., 35-959 RZESZOW, POLAND
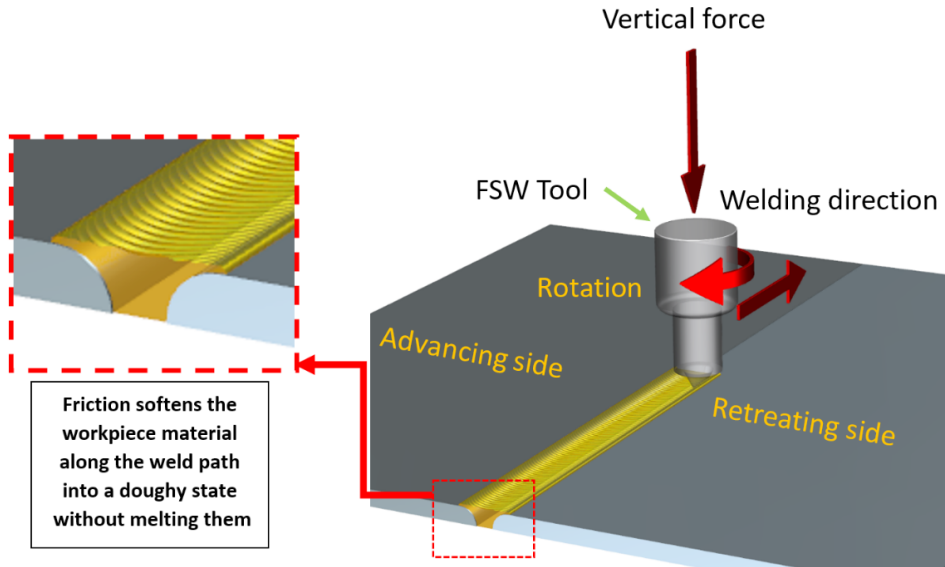
Corresponding author: r.sliwa@prz.edu.pl

Fig. 1. Scheme of FSW process

The aim of the research is to analyze the impact of the type of tool material on the quality of FSW joints. The joints were made using a ceramic tool. The literature review did not find any information on the impact of the tool ceramic material on the quality of FSW joints. The low thermal conductivity of ceramics compared to tungsten carbide or steel tool prevents heat loss from the weld zone through the tool. Direct contact of the FSW tool and the fixture with the weld and the plates causes uncontrolled heat pickup, which affects into the technological parameters of the process and, as a result, the quality of the joints.

2. Experimental procedure

The initial material used in this work is a cold-rolled commercial AA2024-T3 aluminum alloy (AlCu4Mg1/AlCu4Mg2) sheet with the 0.5 mm in thickness. In this investigation, the joining region are carefully cleaned prior to welding. After polished by abrasive paper and cleaning with acetone, several weld plates were subjected to FSW along the rolling direction. The blank sheet dimensions were 180×100 mm [length×width] (Fig. 2a). A backing plate witch two holders constituted the fix-

ture to firmly hold the workpiece (Fig. 2b). Fixing device with workpiece was installed on the plate of piezoelectric Kistler dynamometer shown on Fig. 2a. The FSW experiments were carried out on a special adopted CNC milling machine MAKINO PS95 (Fig. 2b,c) using the welding tool shown on Fig. 3. Cylindrical tool made from ceramic (BlueCer) with geometrical features and process inputs reported in Table 1.

TABLE 1

Inputs used for the experimental set-up of FSW

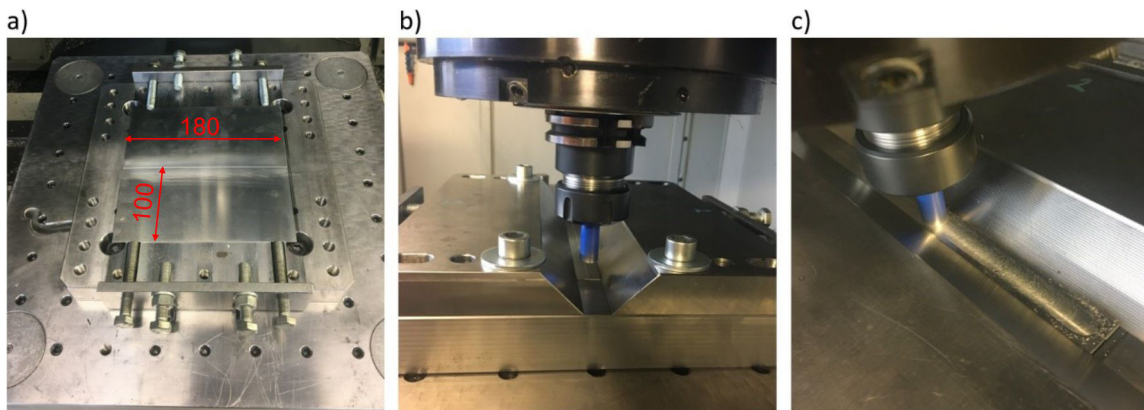| Tool material	Ceramic (BlueCer)
Shoulder diameter D	10 mm
Pin diameter d	3,2 mm
Pin height	0,45 mm
Pin profile	cylindrical
Shoulder profile	Flat
D/d ratio of the tool	3,125
Dwell time	10 s
Penetration depth (tool offset)	0,03 mm

Fig. 2. a) view of workpiece material installed on fixture device; b) view of stand for FSW process; c) the FSW process in action
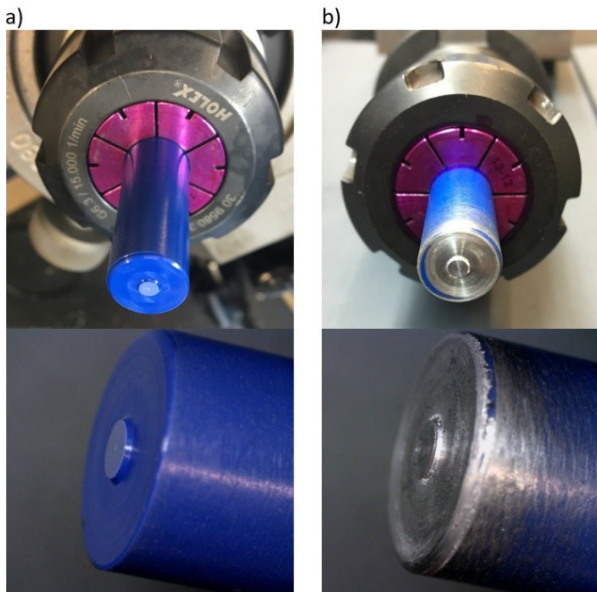
Fig. 3. The tool used in FSW process: a) new tool; b) tool after making 2 m of FSW joints

Tool dimension was adjusted to the material sheet thickness according to algorithm [4] shown in literature. Generally it can be assumed that the ratio of shoulder diameter to pin diameter is around 3. Both the pin and the shoulder of the tool have smooth cylindrical shape. Tool worked without a tilt angle, perpendicular to the surface of the welded material. The butt joint configuration was prepared to produce the joints. Welding has been done on the 180 mm long section. The welding conditions and tool parameters used for welding in this work are listed in Table 2. Shoulder plunge depth (tool offset) was chosen as 0.03 mm.

FSW welding experiments were carried out with constant values of rotational speed 1000 rpm and welding speed from 100 to 200 mm/min. The dwell time was the same for all joints and was 10 s. Tool plunging in and out stages was realized with tool feed rate equal 5 mm/min. In total, 9 FSW welds of 180 mm length were made. The process parameters are submitted in Table 2. The selection of process parameters results from expe-

rience gained while welding various types of metal sheets and literature studies [13]. Visual evaluation of FSW joints showed that they are done properly, have no visible defects, face and ridge surface was smooth and uniform. The selected welds are shown in Fig. 4. During the research, no tool wear was found. Only the aluminum build-up was noticed on the tool that did not affect the process (Fig. 3b).

3. Ultimate tensile strength of the FSW joints

Static tensile test was performed in accordance with PN-EN ISO 6892-1:2009. The tensile tests were carried out on an Zwick/Roell Z 100 universal testing machine, at room temperature. An extensometer with a gauge length of 50 mm was used for strain data acquisition. The results, given by the nominal stress vs. nominal strain curves, were evaluated in terms of the ultimate tensile strength (UTS) and average elongation (AE) in percentage (Fig. 5). The average result for the tensile testing of each welding configuration is presented in figure 6.

The next step was to determine the quality of the FSW weld along the entire length of the sheet. For this purpose, samples for strength tests were prepared from the joined sheet as shown in Figure 7. Samples (13 pcs.) with a width of 12.5 mm were cut from each sheet. On this basis, the quality of the FSW weld in individual sheet locations was checked. Joint 2 exhibited less strength compared to sheet 9 which had the best strength of all. Figure 5 shows the ultimate strengths of individual samples for joint 2 and 9. Figure 6 compare average strength of welded sheets. We conclude that the quality of FSW weld in individual sheet locations is not at the same level. The drop in strength at the beginning of the weld is noticeable. This proves that the FSW process is not fully stable and repeatable. This is related to the process temperature change.

After welding both the strength and elongation of FSW joint reduced. The Ultimate Tensile Strength (UTS) of BM (base material) was obtained to be 460 MPa. Joint efficiency of the FSW joints varied approximately from 89% to 96% (Fig. 6). The
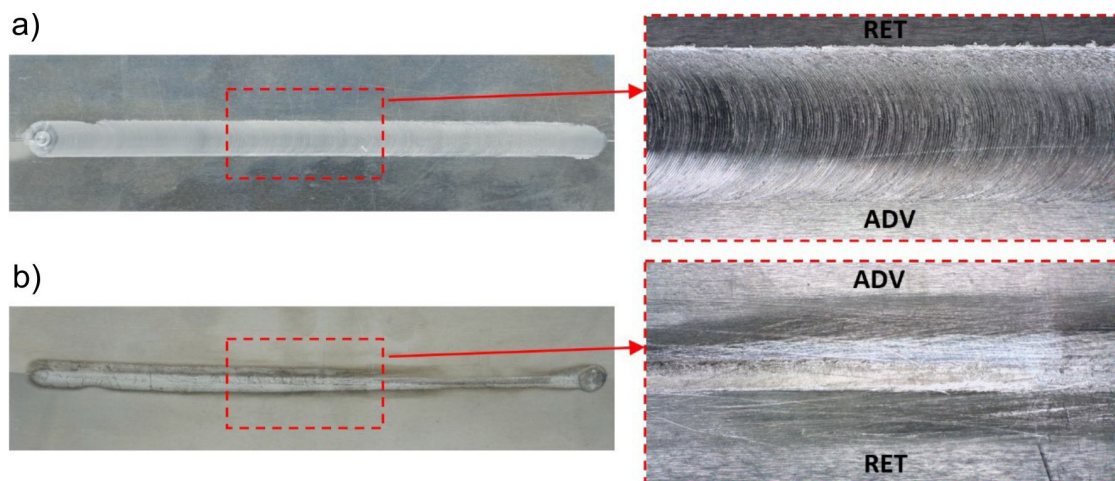

Fig. 4. General view and close-up images showing surface quality of welds performed by a ceramic tool at 1000 rpm and 200 mm/min; a) face side; b) ridge side (ADV-advancing side, RET-retreating side)

Linear FSW technological parameters, joints and parent material (PM) mechanical properties and average experimental results of AA 2024-T3 alloys 0.5 mm in thickness

Weld No.	Rotational speed, ω [rpm]	Welding speed, v [mm/min]	Weld pitch v/ω	UTS [MPa]	Average elongation [%]	Standard deviation	Joint effectiveness [%]
1		100	0,1	411	10,7	9,6	89
2				416	12,2	15,1	90
3		150	0,15	429	14,2	4,1	93
4	1000			422	12,6	7,3	91
5				427	11,2	4,6	93
6				417	12,8	19,2	90
7		200	0,2	424	13,14	13,9	92
8				422	13	13,7	91
9				442	17	6,5	96
PM				460	31		
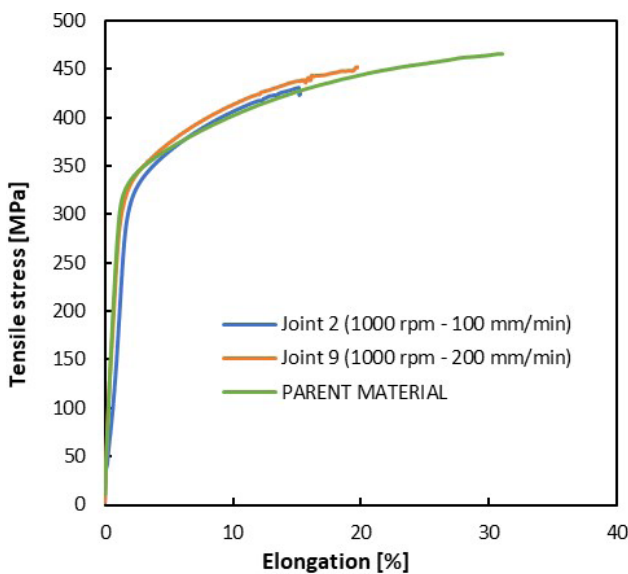
Fig. 5. An example of tensile load – elongation curves for FSW joints and parent material

Fig. 6. Comparison of tensile strengths of parent material and obtained FSW joints; No. 1-9 FSW joints, No. 10-base material

failure of the specimens occurred usually outside of the weld in the heat affected zone (HAZ). It can therefore be assumed that (HAZ) is a so-called structural notch. Nevertheless, the maximum elongation of the weld is only 17% and this was much lower than that of the parent material 31%. This was due to the microstructure of the weld stir zone, which is non-homogeneous along the depth, resulting in a concentration of stress during the tensile testing. Because of that, the crack is effortlessly initiated from the bottom what was presented in [14].

Several welding parameters have been tested in order to achieve the strongest welds using ceramic tools. The most beneficial results was achieved when the welding speed set up on 200 mm/min. We note that the strongest FSW joint has been obtained for the parameters set 9 from the Table 2 for rotational speed 1000 rpm and welding speed 200 mm/min. The effectiveness of FSW joints was on the level 96% when compared to the base material. Further increase the welding speed caused gradual decline in (UTS). The combined role of both the welding speed and rotational rate could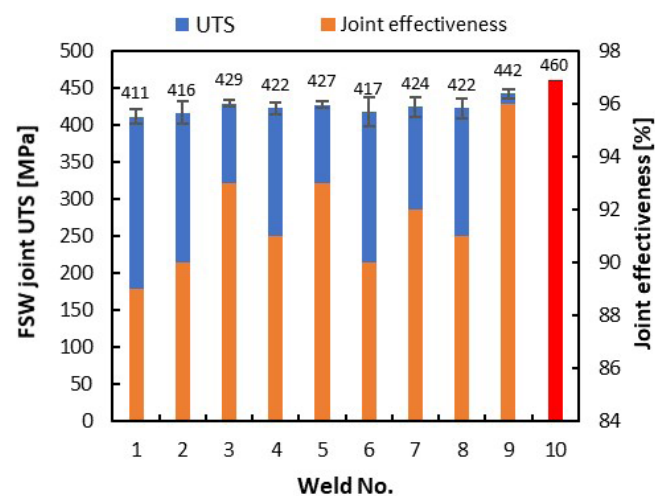 be better represented by the weld pitch (v/ω). The strength of the FSW joint as a function of the weld pitch is plotted in Fig. 8. As the welding pitch increases, the joint ultimate strength increases.

4. Force measurements in FSW process

During the welding process, the changes in welding parameters result in force variations. To fabricate an ideal joint, the main input parameters should be selected appropriately. Regarding the conditions under which the experiments were conducted the ranges of 100-200 mm/min for the welding speed and constant tool rotational speed (1000 rpm), and plunge depth/tool offset (0.02 mm), were found to be the appropriate process settings resulting in defect – free welds. The improper combination of parameters is resulting from insufficient plastic deformation, stirring action and defective welds.

The vertical (Z axis) and horizontal (X,Y axis) forces occurring during linear FSW process was measured by high
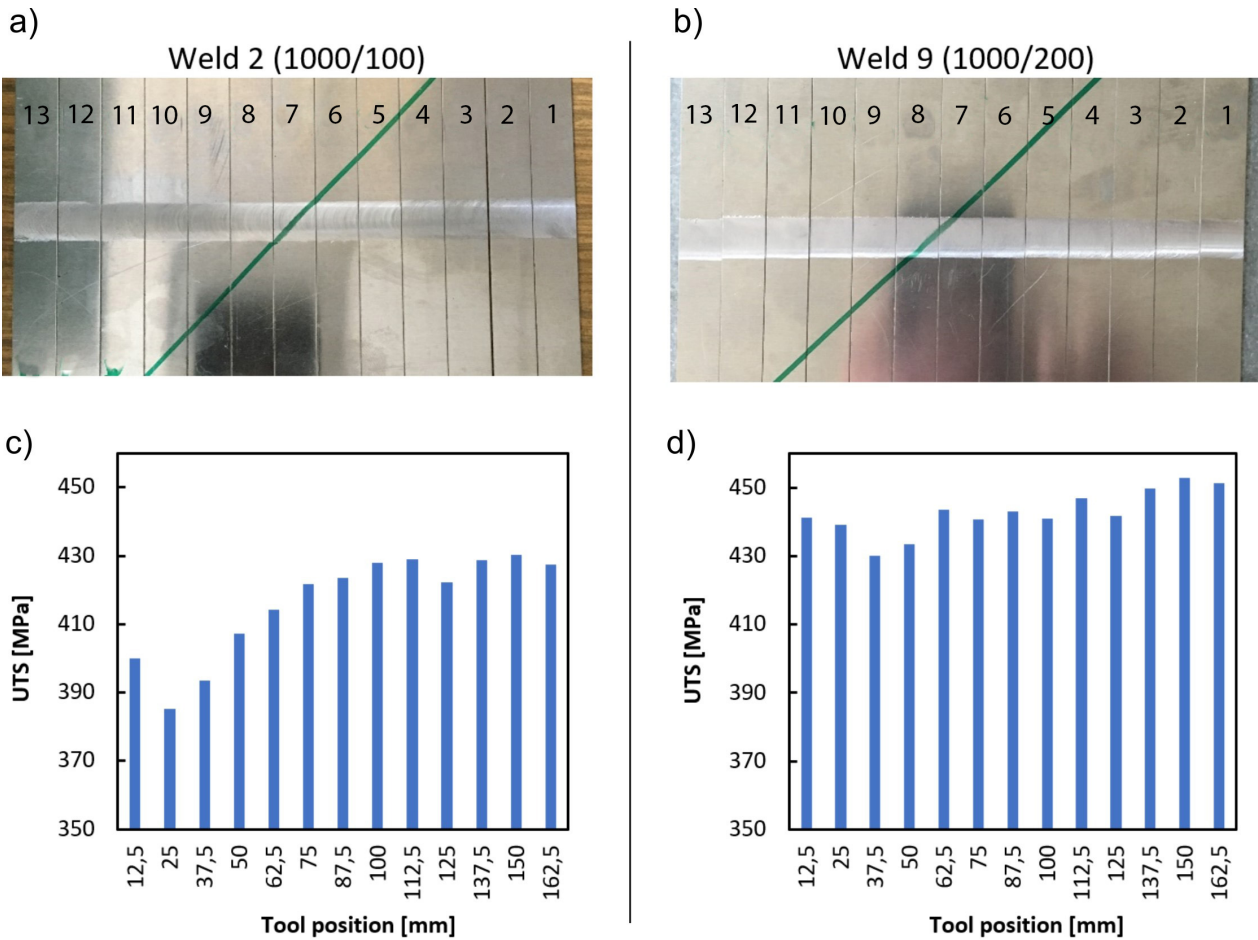
Fig. 7. View of FSW welds with prepared samples – a) and b); c) and d) UTS for sample extracted from various locations of the weld (tool position from edge of the sheet)
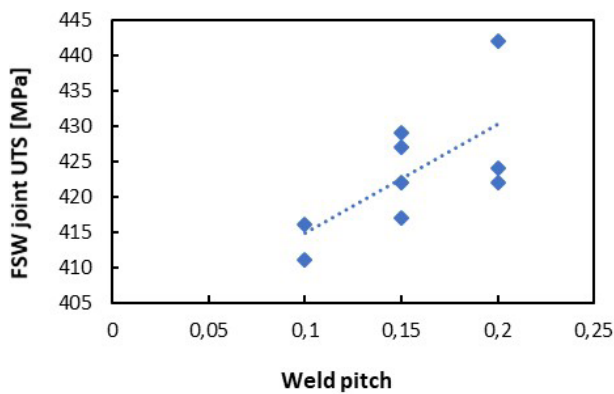

Fig. 8. A comparison of the (UTS) of the AA2024-T3 weld joints as function of the weld pitch (the ratio of welding speed)

sensitive piezoelectric dynamometer developed by Kistler. It consist of four piezoelectric force sensor calibrated in range from 0 to 60 kN in Z axis and 0 to 10 kN in X,Y axis. The force data were acquired with a maximum sample rate per channel of 200 kHZ and 16-bit resolution. The actual sample rate used during the data recording was 1 kHz. Measurement of forces was conducted for all 9 samples. Figure 9a, b shows a typical vertical and horizontal forces versus time curve recorded during FSW. Set 2 belong for the FSW welded with welding speed setup at

100 mm/min and the set 9 made with 200 mm/min. Graphs of force for both cases are similar. Four different stages of FSW process can be recognized: (1) tool plunging, (2) tool dwelling, (3) welding, (4) tool pulling out.

Values of welding forces, both maximum and average, are shown in Table 3. The analysis of welding forces during the FSW process shows that along with the increase in welding power (increase the welding speed) the load capacity of the joint also increases, as shown in Figure 10.

TABLE 3

Comparison of axial (Z) and radial (X, Y) welding force (maximum and average value).

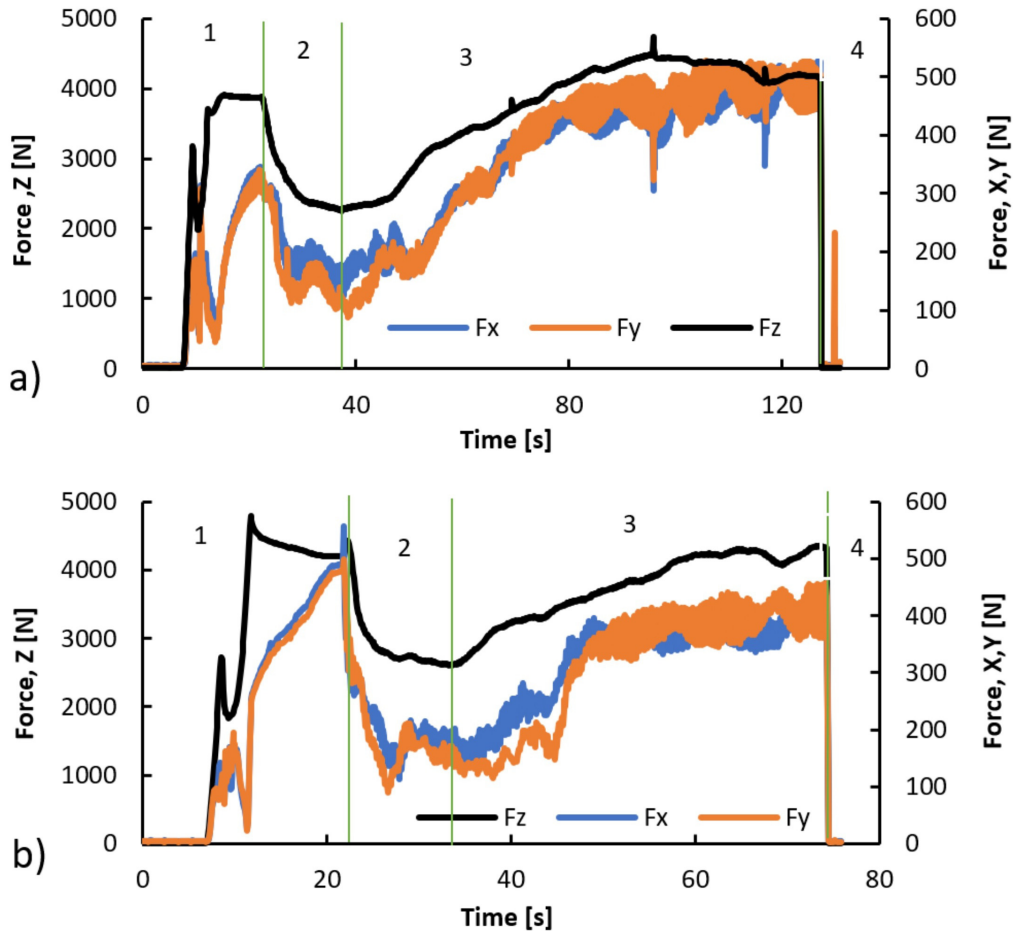| Weld No.	MAX. VALUE [N]			AVERAGE VALUE [N]		
	X	Y	Z	X	Y	Z
1	540	518	4034	321	274	2670
2	527	528	4732	218	202	2742
3	530	467	4314	337	290	3088
4	543	476	4148	264	231	2908
5	508	442	4190	320	264	2540
6	544	509	4424	354	315	2987
7	546	423	4586	286	261	3061
8	532	501	5089	362	298	3158
9	557	499	4793	268	260	3192

Fig. 9. Graph of the axial and translational forces versus time during FSW of 2024-T3 alloy sheet for: a) ω = 2000 rpm, v = 100 mm/min; b) ω = 2000 rpm, v = 100 mm/min witch marked stages: (zone 1) tool plunging, (zone 2) tool dwelling, (zone 3) welding, (zone 4) tool pulling out
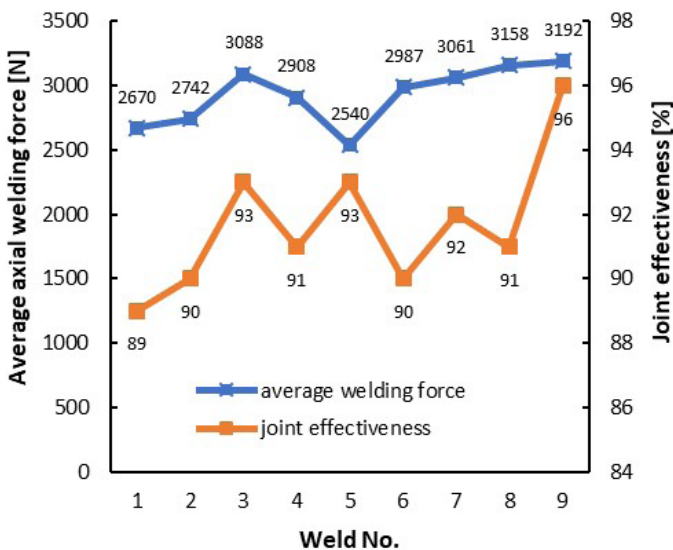

Fig. 10. Comparison of average axial welding force versus joint effectiveness (FSW joints: 1-9)

5. Micro hardness of FSW joints

Material hardness was measured using a Vickers micro hardness tester NEXUS 4303 according to ASTM E382-16.

Applied load equal 1N. Measurements were carried out on a cross-section of the sheet in the area of the weld to approx. 20 mm. For each cross-section, an average of 40 indentations 0.5 mm apart, were made on the weld surface. The measurements scheme was shown in Fig. 11. This provided data from outside the stir zone on each edge of the weld, in order to determine how the welding parameters affected both the stir zone SZ (Stir Zone) and heat affected zone HAZ (Heat Affected Zone). Since AA2024 is a precipitation hardened alloy, changes in the main characteristics of precipitates (i.e. size, volume fraction, composition, distribution, etc.) during and after welding will be the most important phenomena dictating the resulting hardness and strength of the different weld zones. Micro hardness of FSW welds showed the presence of (HAZ), where hardness increase to 128-130 HV from a parent material hardness value of 127 HV. The hardness reduction in SZ is due to the dissolution of Al_3Li precipitates as the (SZ) experiences temperature in range of 200-400°C, which is high enough for dissolution of low thermal stability δ' precipitates what was submitted in [15].

Therefore it is well accepted that the highest hardness value occurs in the (HAZ) and (PM) followed by a gradual decrease across the TMAZ (Thermo Mechanically Affected Zone) and SZ as shown in Fig. 12. This is attributed to more grain refinement in the (SZ) due to dynamic recrystallization and more uniform

distribution of finer reinforcement particles in the weld zone due to FSW action [16]. However, the high temperature in the tool working area leads to secondary grain growth. The lower hardness in (SZ) corresponds to the tool material that does not absorb heat, which causes a local increase in temperature. These conclusions agreed with the Hall-Petch equation (inversely proportional relation between hardness and grain size) and the Orowan hardening mechanism (hardness can be improved if finer particles distribute homogenously) [17]. Generally the differences in microhardness are not large as shown in Table 4.

With the microhardness profiles it is also possible to determine the extent of the different weld zones. As expected the (SZ) has a width of roughly 11 mm which corresponds to the diameter of the tool shoulder.
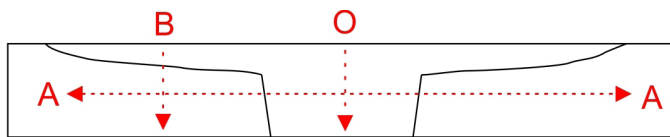

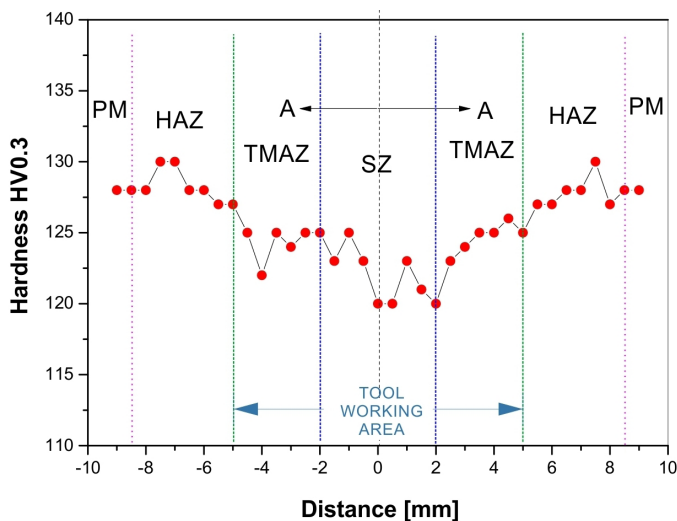
Fig. 11. Scheme of hardness measurement areas

Fig. 12. Microhardness profile of FSW joint

TABLE 4

Hardness of the AA2024-T3 alloy depending on the area – Fig. 11 (average values)

Hardness HV			
Direction A-A	HAZ **126**	SZ **123**	PM **128**
Direction O	Face side **125**	half of the cross-section **125**	Ridge side **125**
Direction B	Face side **124**	half of the cross-section **127**	Ridge side **128**

6. Low-cycles fatigue test of FSW joints

Fatigue testing was performed to ASTM standard E466-07. The specimen for low-cycle fatigue test was made with the fol-

lowing parameters: rotational speed 1000 rpm, welding speed 200 mm/min. Testing was undertaken at eight load levels, specifically 99%, 98%, 95%, 90%, 85%, 80%, 75% and 70% of the load corresponding to the ultimate tensile strength of the material, with three repeat tests at each level. The dimensions of the specimens and load scheme are shown on figure 13. The tests were carried out on the Zwick/Roell Z100 universal testing machine. The displacement speed was 20 mm/min at room temperature which corresponded strain rates equal 3.3×10^{-1} 1/s. The results of from zero pulsing tests are shown in the Table 5 and Fig. 14. The failure of the samples appeared in SZ or TMAZ area.
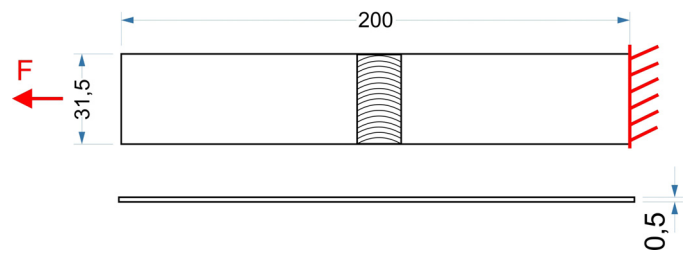

Fig. 13. Uniaxial low-cycles fatigue testing geometry (dimension are in mm) and load scheme

TABLE 5

Low-cycle fatigue test data

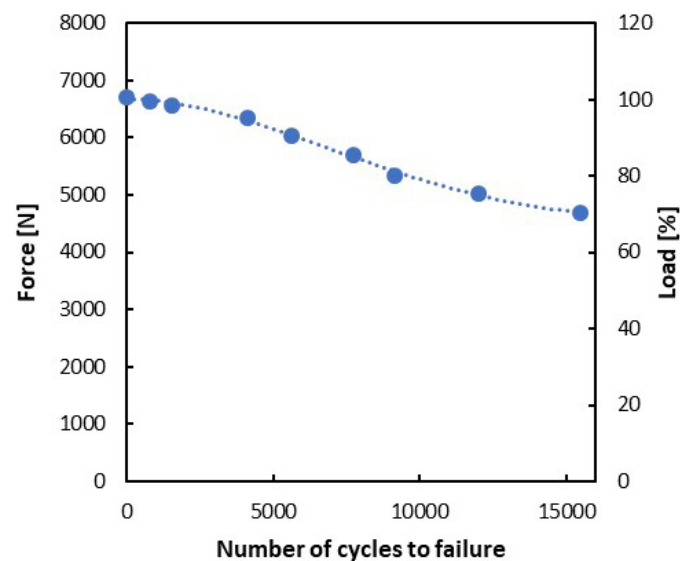| Test no.	Load [%]	Force [N]	Number of cycles
1	100	6700	1
2	99	6633	793
3	98	6566	1531
4	95	6350	4115
5	90	6030	5622
6	85	5695	7746
7	80	5340	9169
8	75	5030	12029
9	70	4690	15478

Fig. 14. Low-cycles fatigue behavior for friction stir welded AA2024-T3 joints

Fatigue tests showed that the obtained FSW joint had a relatively high fatigue strength, taking into account that the load at the level of 70% corresponded to the yield strength of the native material.

7. Microstructure of FSW joint

The observations were carried out directly on the surface of the weld and on the cross-section in a plane perpendicular to the axis of the weld. The test sample was made using standard methods with the use Struers devices. Microscopic examinations were performed on samples digested with Keller's reagent (No. 3 according to ASTM E407-07). Microscopic observations were carried out using light microscopes – stereoscopic Zeiss Stemi C-2000 and metallographic Nikon Epiphot 300.

The macroscopic observations of the weld showed that the surface on the face side is clean, unoxidized, with a metallic light gray color, typical of the aluminum alloy, whereas from the ridge side slight local oxidation was observed. On the face side are visible regular, semicircular lines / traces of the tool, the so-called onion rings, which from the trailing edge side are

less pronounced due to the material being drawn / smeared in the direction of the tool movement (Fig. 15).

Both the macroscopic observations of the weld and the microscopic observations of the cross-section did not reveal any flaws in the area, such as cracks, tearing of the material or other types of discontinuities. The etching process revealed the weld's macro structure – from the side of the leading edge the outline of the weld is clear and contrasts with the material of the sheet, while from the edge of the trailing edge the border is gentler and more blurred (Fig. 16), also allowed for an accurate measurement of its basic parameters – the width of the ridge is 3 mm, while the width of the face 11.2 mm.

The microstructure of the alloy in the area beyond the weld is fine-grained, typical for the precipitation-hardened aluminum alloy (Fig. 17). The microstructure of the sheet in the area of the weld has undergone a severe deformation consisting in considerable fragmentation of the warp grain, with the greatest deformation occurring in the axis of the weld area from both side (Fig. 18).

The welding process caused the change of the alloy microstructure in the weld area and directly adjacent to it (SWC), compared to the sheet metal microstructure, consisting mainly
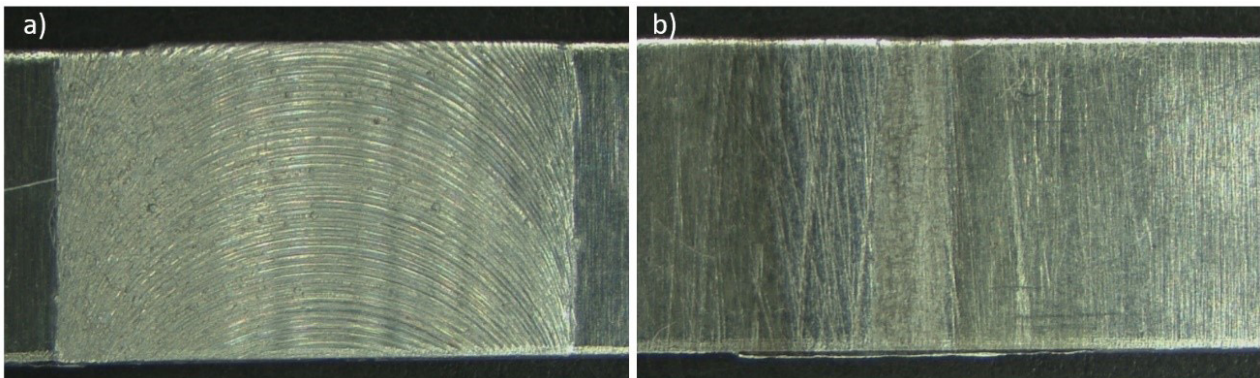

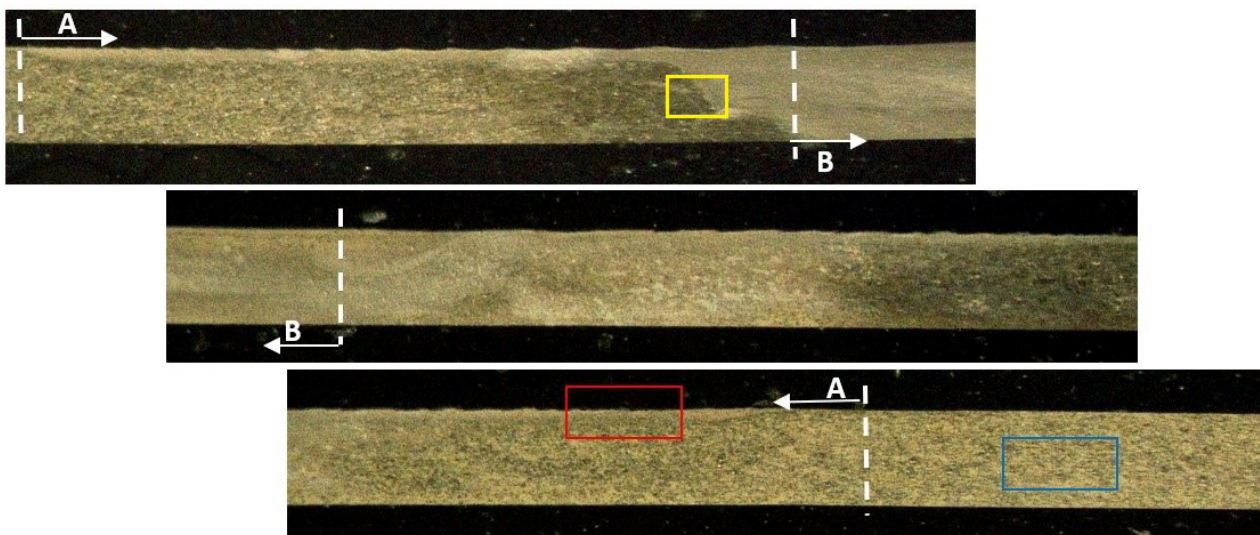Fig.15. Close-up weld view from: face (a) and ridge (b) side

Fig. 16. Macro structure of the FSW weld – width from face side (A-A), from the ridge side (B-B), etched state
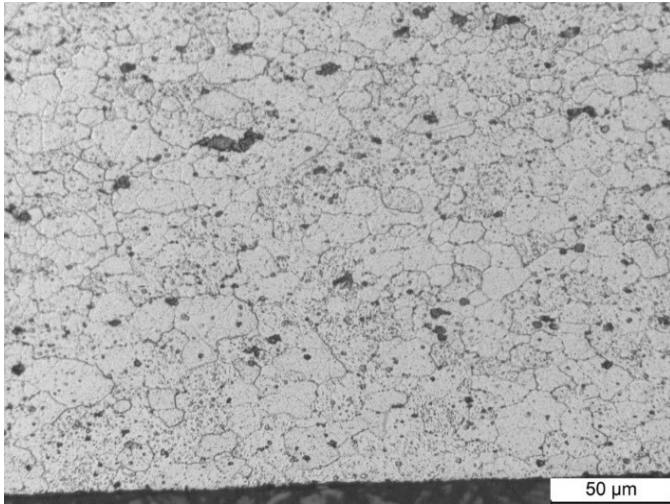
of grain size change – significant grain refinement in the weld area and increase in size in the heat affected zone area (HAZ). Figure 19 shows the interface zone between the fine grain of the stir zone (SZ) and the parent material (PM).

8. Conclusions

The present work investigated the influence of using ceramic tool and different welding speed for friction stir welding on the microstructure as well as on the mechanical properties of AA2024-T3 joints. The friction stir welds were examined through optical microscopy, micro-hardness measurements, tensile testing, low-cycle fatigue tests and welding force measurements. These results indicate that the AA2024-T3 shows very good properties using ceramic tools. Proposing technological

Fig. 17. Microstructure of the parent material area outside the weld (blue frame in figure 16), etched state
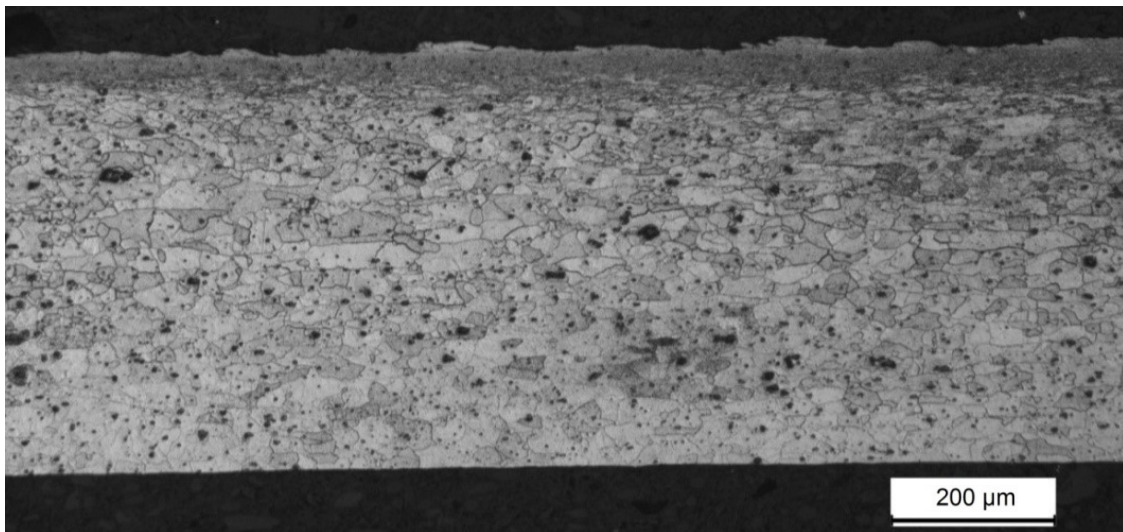

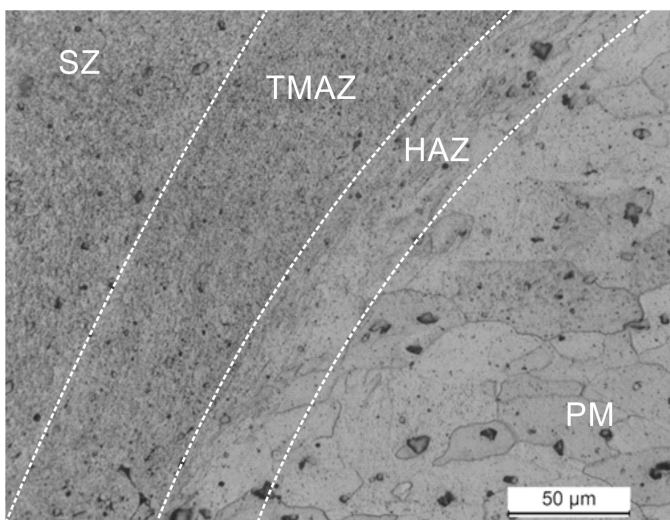Fig. 18. Microstructure of the alloy in the weld area (red frame in figure 16), etched state

Fig. 19. Microstructure of the FSW joint; SZ – stir zone , TMAZ – thermomechanical affected zone, HAZ – heat affected zone, PM – parent material, (yellow frame in figure 16)

parameters guarantee receiving very good quality FSW joints. The main conclusions are as follows:
• The use of a ceramic tool allows to obtain FSW welds with high strength (UTS) up to 96% compared to the base material.
• All demonstrated technological parameters allowed to make a good quality FSW joints.
• Analysis of the strength of the FSW joint as a function of the tool position revealed differences especially in the initial welding phase.
• As the welding force increases, the strength of the FSW joints also increase.
• Used ceramic tool did not show signs of wear after making a 5 m weld.
• The microhardness measurement showed only slight differences in microhardness in the weld and the parent material. Micro hardness from SZ was on average 5% lower compared to base material.

- An increase in the welding pitch increases the strength of the FSW joint.
- During the low-cycle fatigue tests, the sample performed over 15,000 stretching cycles under loaded 70% of breaking force.

REFERENCES

[1]   W.M. Thomas, E.D. Nicholas, J.C. Needham, M.G. Murch, P. Templesmith, C.J. Dawes, Friction Stir Butt Welding, International Patent Application PCT/GB92/02203, GB Patent Application 9125978.8. 6 and US Patent 5,460,317, Dec. 1991.

[2]   S. Guo, L. Shah, R. Ranjan, S. Walbridge, A. Gerlich, Int. J. Fatigue **118**, 150-161 (2019).

[3]   Y. Huang, L. Wan, X. Meng, Y. Xie, Z. Lv, L. Zhou, J. Manuf. Processes **35**, 420-427 (2018).

[4]   Y.N. Zhang, X. Cao, S. Larose, P. Wanjara, Can. Metall. Q. **51** (3), 250-261 (2012).

[5]   Q. Wen, W.Y. Li, W.B. Wang, F.F. Wang, Y.J. Gao, V. Patel, Journal of Mat. Sci. and Tech. **35**, 192-200 (2019).

[6]   B.K. Colligan, Supplement To The Welding Journal **6**, 229-237 (1999).

[7]   S. Xu, X. Deng, A.P. Reynolds, T.U. Seidel, Sci. Technol. Weld. Joining **6** (3), 191-193 (2001).

[8]   R.S. Mishra, Z.Y. Ma, Mater. Sci. Eng. R **50**, 1-78 (2005).

[9]   H. Fujii, L. Cui, M. Maeda, K. Nogi, Mater. Sci. Eng. A **419**, 25-31 (2006).

[10]   S. Vijayan, R. Raju, IJAER **3** (10), 1303-1316 (2008).

[11]   B.S. Kulkarni, S.B. Pankade, S.R. Andhale, C.L. Gothe, Procedia Manuf. **20**, 59-64 (2018).

[12]   N. Balasubramanian, B. Gattu, R.S. Mishra, Sci. Technol. Weld. Joining **14** (2), 141-145 (2009).

[13]   P. Myśliwiec, R.E. Śliwa, R. Ostrowski, Metal Forming **28** (4), 263-280 (2017).

[14]   H. Liu, Y. Hu, C. Dou, D.P. Sekulic, Mater. Charact. **123**, 9-19 (2017).

[15]   H. Sidhar, N.Y. Martinez, R.S. Mishra, J. Silvanus, Mater. Des. **106**, 146-152 (2016).

[16]   O.S. Salih, H. Ou, W. Sun, D.G. McCartney, Mater. Des. **86**, 61-71 (2015).

[17]   P. Periyasamy, B. Mohan, V. Balasubramanian, S. Rajakumar, S. Venugopal, Trans. Nonferrous Met. Soc. China **23** (4), 942-955 (2013).